Mon. Not. R. Astron. Soc. **360,** 380–389 (2005) doi:10.1111/j.1365-2966.2005.09048.x

The *XMM–Newton* view of Mrk 3 and IXO 30

Stefano Bianchi,[1,2,3]★ Giovanni Miniutti,[3] Andrew C. Fabian[3] and Kazushi Iwasawa[3]

[1]*XMM–Newton Science Operations Centre, European Space Astronomy Centre, ESA, Apartado 50727, E-28080 Madrid, Spain*
[2]*Dipartimento di Fisica, Università degli Studi Roma Tre, Via della Vasca Navale 84, I-00146, Roma, Italy*
[3]*Institute of Astronomy, Madingley Road, Cambridge CB3 0HA*

Accepted 2005 March 23. Received 2005 March 8; in original form 2004 December 16

ABSTRACT

We present the analysis of the *XMM–Newton* European Photon Imaging Camera (EPIC) pn spectrum of the Seyfert 2 galaxy Mrk 3. We confirm that the source is dominated by a pure Compton reflection component and an iron Kα line, both produced as a reflection from a Compton-thick torus, likely responsible also for the large column density ($1.36^{+0.03}_{-0.04} \times 10^{24}$ cm^{-2}) which is pierced by the primary power law only at high energies. A low inclination angle and an iron underabundance of a factor $\simeq$0.82, suggested by the amount of reflection and the depth of the iron edge, are consistent with the iron Kα line equivalent width with respect to the Compton reflection component, which is 610^{+30}_{-50} eV. Moreover, the iron linewidth, $\sigma = 32^{+13}_{-14}$ eV, if interpreted in terms of Doppler broadening due to the Keplerian rotation of the torus, puts an estimate to the inner radius of the latter, $r = 0.6^{+1.3}_{-0.3} \sin^2 i$ pc. Finally, two different photoionized reflectors are needed to take into account a large number of soft X-ray emission lines from N, O, Ne, Mg, Si, Fe L and the Fe XXV emission line at $6.71^{+0.03}_{-0.02}$ keV. RGS spectra show that the soft X-ray spectrum is dominated by emission lines, while the underlying continuum is best fitted by an unabsorbed power law with the same photon index as the primary continuum, produced as a reflection by a photoionized material with a column density of a few $\times 10^{22}$ cm^{-2}. We also present the first X-ray spectrum of the *ROSAT* source IXO 30, which shows a huge iron line at $6.5^{+0.3}_{-0.2}$ keV and is well represented either by an absorbed power law with $\Gamma \simeq 1.8$ or by bremsstrahlung emission at a temperature of $7.5^{+2.1}_{-1.6}$ keV. Its spectral properties point to a likely identification in terms of a weak Galactic cataclysmic variable, but the lack of any optical counterpart precludes excluding other possibilities, such as an ultraluminous X-ray source at the distance of Mrk 3.

Key words: galaxies: active – galaxies: Seyfert – X-rays: individual: Mrk 3 – X-rays: individual: IXO 30.

1 INTRODUCTION

Mrk 3 ($z = 0.0135$) is a prototypical Seyfert 2 galaxy, the optical broad lines of which are seen only in polarized light (Miller & Goodrich 1990; Tran 1995). As soon as it was observed in X-rays by *Ginga*, it was clear that the source was heavily absorbed and presented a strong iron Kα line (Awaki et al. 1990, 1991). Moreover, a soft excess was detected by *Einstein* (Kruper, Canizares & Urry 1990) and *ROSAT* (Turner, Urry & Mushotzky 1993). Iwasawa et al. (1994) suggested that it could originate in an extended region, likely dominated by scattering of the intrinsic continuum, on the basis of the *ASCA* observation, which also indicated a significant flux variability above 4 keV with respect to the previous data.

The availability of broad-band observations, due to *RXTE* (Georgantopoulos et al. 1999) and, in particular, *BeppoSAX* (Cappi et al. 1999), allowed these authors to disentangle three different components: a heavily absorbed power law, an unabsorbed Compton reflection component associated with the iron line and a constant soft X-ray emission. The latter component was later found to be spatially extended along the [O III] cone and likely produced in a warm photoionized material, as shown by the high spatial and energy resolution observation by *Chandra* (Sako et al. 2000).

In this paper, we analyse the *XMM–Newton* European Photon Imaging Camera (EPIC) pn and the RGS spectra of Mrk 3, comparing the results with the long X-ray history of the source, with the aim of estimating some properties of the material around its nucleus.

2 DATA REDUCTION

2.1 *XMM–Newton*

Mrk 3 was observed by *XMM–Newton* between 2000 October 19 and 20, with all the EPIC CCD cameras, the pn (Strüder et al. 2001)

★E-mail: Stefano.Bianchi@sciops.esa.int

and the two MOS (Turner et al. 2001), operating in full frame and medium filter. This paper deals only with pn data, the count rate of which is well below the maximum for 1 per cent pile-up (see table 3 of Ehle et al. 2003). SAS 6.0.0 was used to reduce the data, with a total net exposure time of 52 ks, after screening for intervals of flaring particle background, applying the procedure to maximize the signal-to-noise ratio introduced by Piconcelli et al. (2004). An extraction radius of 40 arcsec was used for the single and double pattern spectra. After a consistency check by fitting the two spectra separately, we decided to extract a single spectrum, with all patterns from 0 to 4. A weak source is apparent in the pn image just outside our extraction region. However, its flux (measured from the *Chandra* spectrum; see below) is completely negligible with respect to Mrk 3. RGS1 and RGS2 spectra of Mrk 3 were also extracted, adopting standard procedures, with total exposure times of 60 and 58 ks, respectively.

Finally, another source lies at $\simeq$1.6 arcmin from the nucleus, corresponding to *ROSAT* source IXO 30 (Colbert & Ptak 2002). We extracted EPIC pn, MOS1 and MOS2 spectra for this object, adopting extraction radii of 19 arcsec, for total exposure times of 47, 49 and 52 ks, respectively, again after applying the Piconcelli et al. (2004) procedure. In the following fits, the two MOS spectra were furthermore added to a single spectrum. Moreover, in order to study the flux variability of this source, we analysed all the available EPIC pn observations of the Mrk 3 field (listed in Table 5), with the only exception of observation 0009220901, where IXO 30 lies partly in the chip gap.

2.2 *Chandra*

Chandra observed Mrk 3 with the ACIS-S HETG between 2000 March 18 and 19, for $\simeq$100 ks. The data were already analysed by Sako et al. (2000). However, in order to better compare them to pn data, we re-extracted first-order HEG and MEG spectra with CIAO 3.1 and CALDB 2.27, following standard procedures.

The zeroth-order spectrum of a source ($\alpha_{2000} = 06^{\rm h}15^{\rm m}29\overset{\rm s}{.}7$, $\delta_{2000} = +71^\circ01'40\overset{''}{.}9$) lying at $\simeq$45 arcsec from the nucleus was extracted, to verify if it could contaminate the pn spectrum (see above). An extraction region with a radius of 3 arcsec was used. The resulting spectrum has a 2–10 keV flux of $\simeq 2.5 \times 10^{-14}$ erg s^{-1}, thus being 200 times weaker than Mrk 3.

Finally, the zeroth-order spectrum of IXO 30 ($\alpha_{2000} = 06^{\rm h}15^{\rm m}15^{\rm s}$, $\delta_{2000} = +71^\circ02'05''$) was also extracted, adopting an extraction region with a radius of 3 arcsec.

All spectra were analysed with XSPEC 11.3.1. In the following, errors correspond to the 90 per cent confidence level for one interesting parameter ($\Delta\chi^2 = 2.71$), where not otherwise stated. The cosmological parameters used throughout this paper are $H_0 = 70$ km s^{-1} Mpc^{-1}, $\Lambda_0 = 0.73$ and $q_0 = 0$.

3 DATA ANALYSIS

3.1 Temporal behaviour

Fig. 1(a) shows the EPIC pn light curve of Mrk 3, along with the light curve of the background. We can conclude that there is no evidence for significant variability during the observation. Moreover, soft and hard X-ray light curves are plotted in Fig. 1(b), along with their ratio. Again, taking into account systematic errors due to the subtraction of the background, no variability is apparent in the observation. As a consequence, we use the whole available exposure time in the following spectral analysis.

3.2 Spectrum

We fitted the 0.5–13 keV spectrum with the model adopted by Cappi et al. (1999) for the broad-band *BeppoSAX* data, which includes a strongly absorbed power law and the components arising from reprocessing of this primary continuum from a Compton-thick material, which is a pure Compton reflection with the same photon index (model PEXRAV; Magdziarz & Zdziarski 1995) and an iron Kα line. Moreover, a steeper, unabsorbed, power law is used to model the soft excess. A column density of 8.46×10^{20} cm^{-2} was included in the model, to take into account the Galactic absorption (Dickey & Lockman 1990).

The resulting fit is unacceptable – $\chi^2 = 1074/251$ degrees of freedom (d.o.f.) – mainly because of large residuals in the soft X-ray spectrum, likely due to emission lines. Moreover, the index of the softer power law is quite steep ($\simeq$3), so that it is not easy to assess its physical origin. Therefore, we examined the RGS spectra, before improving the pn fit. We have found that the soft X-ray spectrum is dominated by emission lines, in particular O VII and O VIII Kα lines

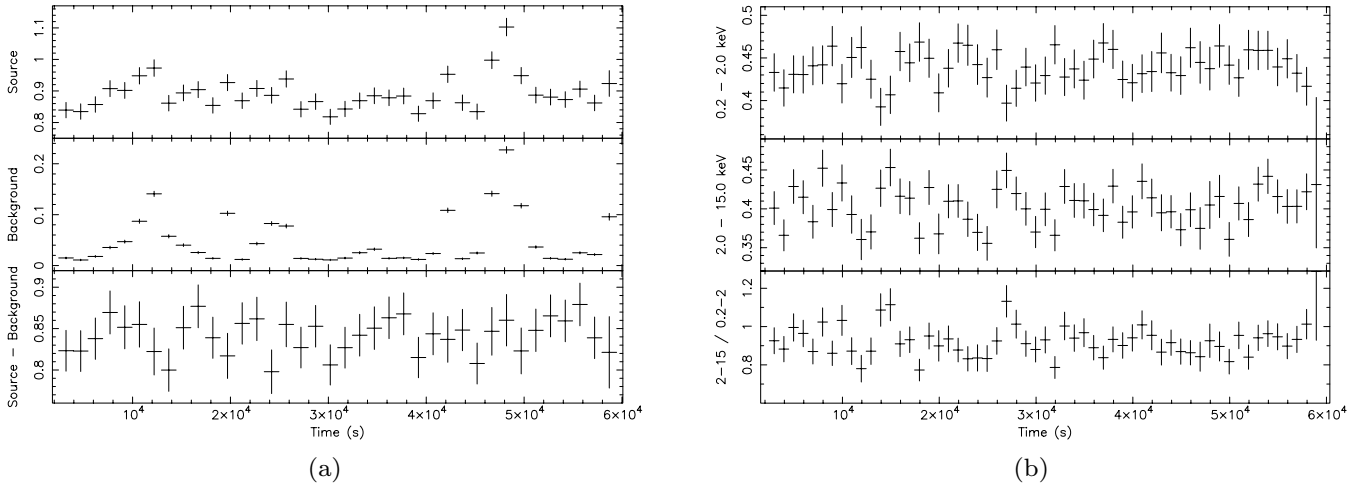

(a) (b)

Figure 1. (a) Upper: light curve of the adopted extraction region for Mrk 3. Middle: light curve for the background, with count rates rescaled to the area of the source extraction region. Lower: background-subtracted light curve of Mrk 3. (b) Upper: 0.2–2.0 keV background subtracted light curve for Mrk 3. Middle: 2.0–15.0 keV background subtracted light curve for Mrk 3. Lower: the ratio of the latter to the former.

Table 1. Best-fitting parameters for the continuum (see text for details.)

$N_{\rm H}$ (cm^{-2})	$1.36^{+0.03}_{-0.04} \times 10^{24}$
Γ	1.77 ± 0.01
$A_{\rm Fe}$	$0.82^{+0.10}_{-0.08}$
$\cos i$	0.45[a]
$F_{0.5-2\,\rm keV}$ (erg cm^2 s^{-1})	6.3×10^{-13}
$F_{2-10\,\rm keV}$ (erg cm^2 s^{-1})	5.9×10^{-12}
$L_{0.1-150\,\rm keV}$ (erg s^{-1})	1.1×10^{44} [b]
χ^2/d.o.f.	249/208

[a] XSPEC default value.
[b] Absorption-corrected extrapolated luminosity.

between 0.5 and 0.7 keV. Including these lines greatly improves the soft X-ray fit of the lower-resolution pn spectrum. We identified each single line with known transitions: when the identification was likely affected by a blend of lines, we tried to include each line in the model, but only when these features improved the reduced χ^2. A power-law component is still required by the data, but now its photon index can be kept fixed to that found for the primary continuum. The final fit is good ($\chi^2 = 249/208$ d.o.f.): the continuum parameters are shown in Table 1, while a detailed discussion on the emission-line spectrum is deferred to Section 4. Figs 2(a) and (b) show the spectrum and the adopted best-fitting model.

The power-law index of the primary continuum and the local absorbing column density are well constrained, the two values being 1.77 ± 0.01 and $1.36^{+0.03}_{-0.04} \times 10^{24}$ cm^{-2}. An interesting result from the fit is a hint of iron underabundance, the best-fitting value being $0.82^{+0.10}_{-0.08}$ (with respect to the solar abundances measured by Anders & Grevesse 1989). However, this result must be taken with caution, because this parameter is actually calculated on the basis of the iron edge depth of the Compton reflection continuum, which also depends greatly on the primary power-law index and the inclination angle.

4 DISCUSSION

4.1 Torus

The Compton reflection component and the strong iron Kα line are clear signatures of reflection from a Compton-thick, fairly neutral, material. It is then natural to assume that the absorber and the reflector are one and the same material, the torus, as usually found in other Compton-thick Seyfert galaxies. It is interesting to note that we also detected a line consistent with emission from Si less ionized than Si VIII (see Table 2), thus likely being another product of reflection from the torus. This feature was also found in the *Chandra* spectrum (Sako et al. 2000).

4.1.1 Compton reflection

The 2–10 keV flux of the Compton reflection component only is 3.4×10^{-12} erg cm^2 s^{-1}, completely consistent with the 3.3×10^{-12} erg cm^2 s^{-1} measured by the *Chandra* observation, performed seven months before. To check for variability in past X-ray observations, we can compare the 2–10 keV total flux reported in Table 1, which by far is dominated by the reflection component (see Fig. 2b). The 1997 *BeppoSAX* observation measured a flux of 6.5×10^{-12} erg cm^2 s^{-1} (Cappi et al. 1999), slightly larger than that of the EPIC pn, the difference probably lying in the brighter intrinsic continuum of the source at that time (see below). Indeed, Cappi et al. (1999) performed a detailed comparison between their data set and the *Ginga* and *ASCA* observations, concluding that there was evidence of a variable component above the iron line energy and a constant one below.

This is also supported by some indications that the intrinsic, unabsorbed luminosity (0.1–150 keV) of Mrk 3 changed between the *XMM–Newton* and *Chandra* observations and with respect to the *BeppoSAX* observation, the values being 1.1×10^{44}, 0.8×10^{44} and 1.3×10^{44} erg s^{-1}, respectively.[1] However, it should be stressed that this luminosity is driven by the normalization of the strongly absorbed power law, so the measures with *XMM–Newton* and, in particular, *Chandra* are much less reliable than that obtained with the broad-band spectrum of *BeppoSAX*.

Finally, an estimate of the angle i can be made on the basis of the amount of Compton reflection with respect to the incident nuclear continuum, which is quite large ($R \simeq 1$; Cappi et al. 1999), thus requiring an inclination not very high to avoid self-obscuration of the torus.

4.1.2 Iron Kα line

A prominent iron Kα line is present around 6.4 keV. However, its equivalent width (EW) with respect to the Compton reflection component, being 610^{+30}_{-50} eV, falls short of that expected, which should be larger than 1 keV (see, for example, Matt, Brandt & Fabian 1996). Two factors can contribute in reconciling the observed value with the theoretical value. One is a small inclination angle, because the iron line EW increases with this parameter. The other is iron underabundance: the dependence of EW with this parameter is almost linear for $A_{\rm Fe} < 1$ (Matt et al. 1996). Both these requirements are satisfied by the Compton reflection component properties, which arise in the same material: the value of R is consistent with low inclination angles (see Section 4.1.1) and the iron edge depth suggests an iron underabundance of a factor of $\simeq$0.82 (see Section 3).

The iron Kα width is actually resolved in the EPIC pn spectrum, with $\sigma = 32^{+13}_{-14}$ eV. Even if this measure is taken with care because it is well below the instrument resolution, it is interesting to note that it is fully compatible with the value found by *Chandra*, which is $\sigma = 28^{+11}_{-7}$ eV. The observed iron linewidth can be in principle explained by several means.

One effect that should, in principle, be taken into account is that the neutral iron line is indeed composed of a doublet, Kα_1 at 6.404 keV and Kα_2 at 6.391 keV, with a flux ratio of 2:1 (Bearden 1967). The difference between the two lines, being lower than the spectral resolution of present X-ray detectors, is generally ignored and a weighted mean of 6.400 keV is commonly used. Yaqoob et al. (2001) have already noted that a fit with two Gaussian lines does not vary significantly the measure of the total linewidth in *Chandra* gratings data. We performed the same test with our high statistics EPIC pn spectrum, fitting the neutral iron line with a Kα_1 and a Kα_2, whose energies and relative intensities were frozen to the atomic values, while their widths were constrained to vary together. The resulting, common width is $\sigma = 35^{+14}_{-16}$ eV, in full agreement with the value found with a single Gaussian line.[2]

[1] The latter two values are those reported by Sako et al. (2000) and Cappi et al. (1999), corrected to have the same choice of cosmological parameters adopted in this paper.
[2] Note that in order to achieve a fit statistically equivalent to that with a single Gaussian line (whose best-fitting energy was significantly higher than that

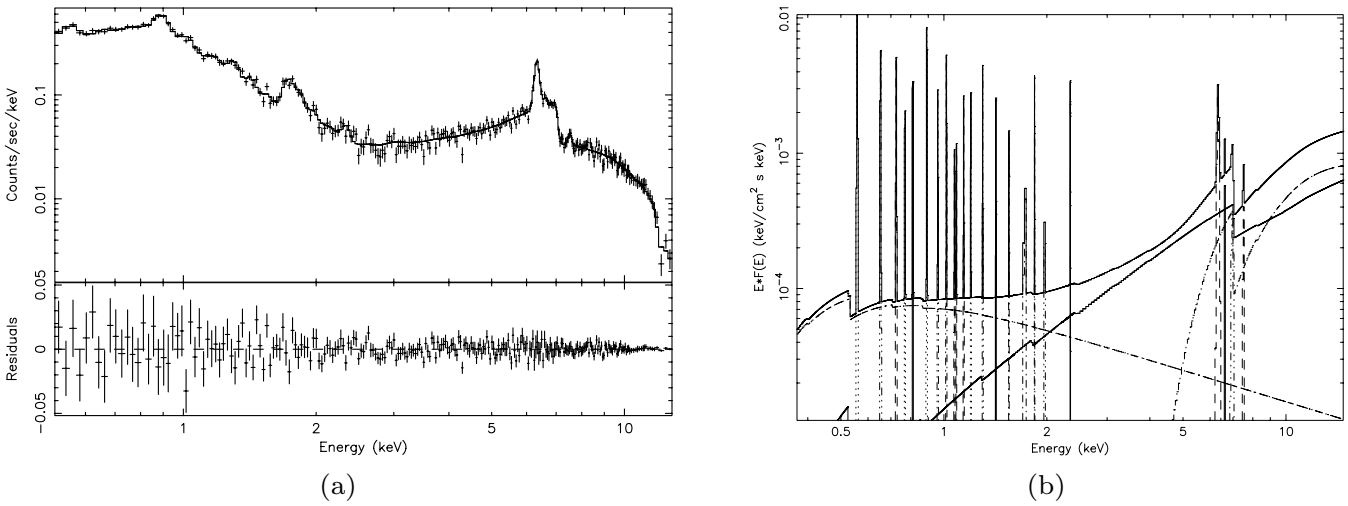

Figure 2. (a) Best-fitting model and residuals for the EPIC pn spectrum. (b) The adopted model plotted as $EF(E)$.

Table 2. List of the emission lines included in the best-fitting model, originating from a fairly neutral material, likely the torus.

Energy (keV)	Flux[a]	Id.	E_T[b] (keV)
$1.744^{+0.018}_{-0.002}$	0.7 ± 0.1	Si I–VIII Kα	1.740–1.769
6.415 ± 0.006	3.8 ± 0.2	Fe XIII–XVI Kα	6.411–6.424
7.06[c]	0.5 ± 0.2	Fe I–XVI Kβ	7.058

[a] 10^{-5} photon cm^{-2} s^{-1}.
[b] Theoretical energies for the transitions (data from NIST; Ralchenko et al. 2004, and references therein).
[c] Fixed.

On the other hand, because the line is produced by reprocessing from a Compton-thick material, a Compton shoulder (CS) is expected on theoretical grounds (Matt 2002), as a result of Compton scattering of the line photons on the same material where they originate. Indeed, the iron line profiles of Circinus and NGC 1068 are successfully modelled with a narrow core and a CS, both in *XMM–Newton* and *Chandra* spectra (Bianchi et al. 2002; Molendi, Bianchi & Matt 2003; Ogle et al. 2003; Matt et al. 2004), with a better statistical significance with respect to a single Gaussian line with a resolved width. Therefore, another possibility is that the observed FWHM is the result of a bad modelling of the overall profile, which does not include the CS. To parametrize this component, we added a further Gaussian line, with centroid energy at 6.3 keV and $\sigma = 40$ eV (Matt 2002). The CS is not required on statistical grounds ($\Delta\chi^2 \simeq 0$ for one d.o.f. less), but the CS flux, even if low, is consistent with production from a Compton-thick material, being 10^{+9}_{-6} per cent of the line core, and the iron linewidth is now unresolved (the upper limit being 50 eV). We then tested whether this model applies well also to the *Chandra* HETG data. However, this is not the case. An unresolved line core plus a CS gives a significantly worse fit with respect to a single, resolved Gaussian ($\Delta\chi^2 = 13$ for the same d.o.f.). On the other hand, if the line core width is left free to vary (with a best-fitting value of $\sigma = 29^{+10}_{-8}$), we obtain an upper limit to the CS flux of 13 per cent, still compatible with the expectations, but not explaining the FWHM of the line.

A more likely possibility is that we are not observing a line from purely neutral iron. If this is the case, the iron Kα line is expected to be actually the blend of a number of emission features from different ionic species, each composed of a doublet, whose transitions are separated by energies of tens of eV. Indeed, the best-fitting value of the centroid energy for the line in the EPIC pn spectrum suggests that iron is ionized in the range Fe XIII–XVI (House 1969). However, the Kβ/Kα flux ratio is $0.12^{+0.06}_{-0.05}$. This value depends not only on the ratio between the fluorescence yields of the two transitions (1 : 8), but also on the different total flux of the continuum and photoabsorption cross-sections at the energies of the two lines. To account for all these effects, Molendi et al. (2003) used the Basko (1978) formulae and obtained for neutral iron a ratio of 0.155–0.160, depending on the inclination angle. Therefore, the measured value in Mrk 3, albeit smaller than the expected value, is fully consistent with a production from neutral iron. Moreover, the Kβ fluorescent yield decreases with the ionization stage, until it becomes null for Fe XVII, when the M shell is completely void and the transition is impossible. Therefore, taking into account the above-mentioned value for neutral iron and scaling it with the fluorescent yields calculated by Kaastra & Mewe (1993), we can estimate that the observed value for the Kβ/Kα flux ratio is appropriate for Fe X–XI, but is inconsistent with iron more ionized than Fe XII–XIII, just marginally in agreement with the centroid energy of the line as observed by the pn.

Finally, if we assume that the torus rotates around the black hole (BH) with a Keplerian velocity, it is easy to show that the expected FWHM for a line produced in its inner walls is approximately $2v_k \sin i \simeq 1300(M_8/r_{pc})^{1/2} \sin i$ km s^{-1}, where the mass is in units of 10^8 M$_\odot$, the inner radius in parsec and i is the angle between the torus axis and the line of sight. The BH mass of Mrk 3 is estimated by means of stellar velocity dispersion to be 4.5×10^8 M$_\odot$ (Woo & Urry 2002). This means that the expected FWHM for the iron line in this source is $2770\, r_{pc}^{-1/2} \sin i$ km s^{-1}. Therefore, the linewidth we measure with the EPIC pn, corresponding to FWHM $= 3500^{+1400}_{-1500}$ km s^{-1} if due to Doppler broadening, puts an estimate on the inner radius of the torus: $r = 0.6^{+1.3}_{-0.3} \sin^2 i$ pc. A choice of 30° or 60° leads to central values of 0.3 and 0.5 pc, respectively, for the inner radius.

of neutral iron), we froze the energy separation between the two transitions (13 eV, appropriate for neutral iron), but allowed the Kα_1 energy to vary. The resulting best-fitting value for the Kα_1 energy is around 6.418 keV, i.e. well above that expected for Fe IX (see, for example, Palmeri et al. 2003, for the theoretical energies of the iron doublet for some Fe ions).

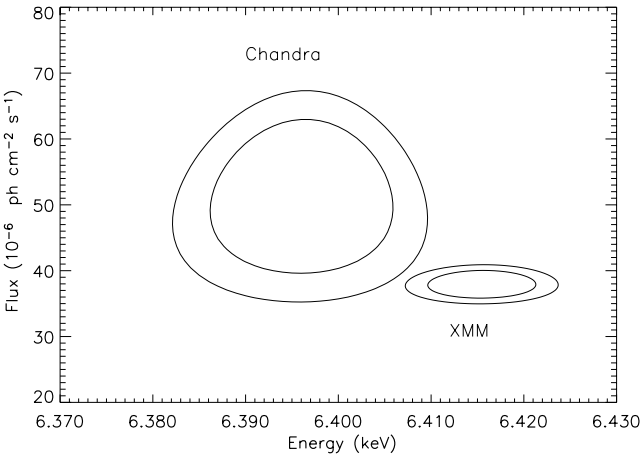

Figure 3. Energy versus flux contour plot for the 'neutral' iron Kα line.

Moreover, there is a marginal indication that the line flux and energy actually changed between the *Chandra* and *XMM–Newton* observations. In Fig. 3 the contour plots for the iron line energy versus flux are shown for both spectra, showing that the two curves are not consistent with each other at the 90 per cent confidence level (for two interesting parameters). Even if the reason for this discrepancy is more likely to be found in a less than perfect calibration of the two instruments [as may be the case in other high statistics EPIC pn spectra of active galactic nuclei (AGNs); see, for example, Molendi et al. 2003; Matt et al. 2004], it may be a good exercise to understand if such a variation is indeed possible, by estimating the expected photoionization time for the neutral iron present in the torus.

The photoionization time can be expressed in a simplified way, as done by Reynolds et al. (1995). The formula they estimated for O VII can also be used in our case, rescaling for the photoionization cross-section and the threshold energy appropriate for neutral iron (see Verner & Yakovlev 1995), so that

$$t_{\rm ph} \simeq 1200\, R_{16}^2 L_{43}^{-1}\ {\rm s} \qquad (1)$$

where $R = 10^{16}\, R_{16}$ cm is the distance of the material from a source with ionizing luminosity ($E > 13.6$ eV) of $L = 10^{43}\, L_{43}$ erg s^{-1}. Adopting an approximate ionizing luminosity of 10^{44} erg s^{-1} (see Table 1), we find that, for a distance of the torus of 1 pc, the resulting $t_{\rm ph}$ is of the order of 10^7 s, i.e. approximately four months. This means that a variation of the photoionization structure of the inner wall of the torus is perfectly reasonable in a time-span of seven months, which separates the two observations.

4.2 Ionized reflectors

4.2.1 Soft X-ray spectrum

The analysis of the RGS spectra shows that the soft X-ray EPIC pn spectrum of Mrk 3 is dominated by emission lines, in particular from O VII and O VIII Kα between 0.5 and 0.7 keV (see Fig. 4). Therefore, we included these lines in the fit with the pn data and added a further power-law component to model the soft X-ray continuum. There is no need now for a very steep power law, as was found in *BeppoSAX* (Cappi et al. 1999) and in our preliminary analysis of the pn spectrum. Instead, a power law with the same photon index as the primary continuum best fits the continuum underlying both the RGS and the EPIC pn emission-line spectra. This component is most likely due to scattering of the primary continuum by a photoionized,

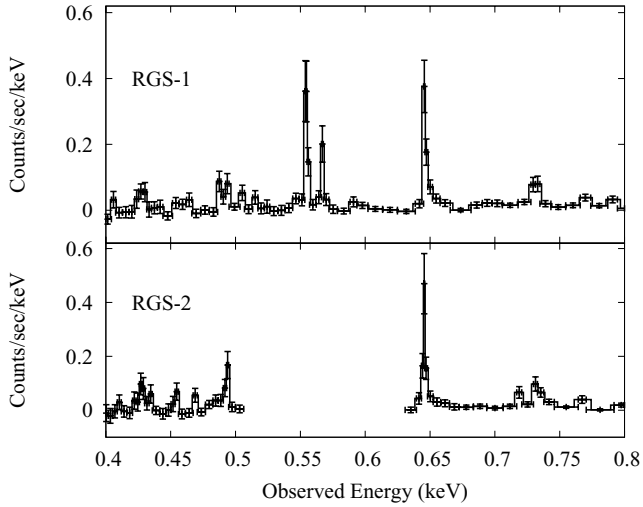

Figure 4. The RGS spectrum of Mrk 3 between 0.4 and 0.8 keV.

Compton-thin gas. Indeed, an estimate of the column density of this material can be calculated on the basis of the ratio between the fluxes of the reflection component and the primary emission, which is $\simeq$1 per cent. Assuming a covering factor of 0.5, just to have an order of magnitude estimate, the column density of the photoionized gas would be approximately 3×10^{22} cm^{-2}. As already noted by Iwasawa, Maloney & Fabian (2002) and Guainazzi et al. (2004, but see also references therein), it may well be that low-resolution spectra of highly absorbed Seyfert galaxies are often affected by a blending of strong emission lines which mimic a continuum component, and only high-resolution spectroscopy can unveil the real nature of this kind of soft excess.

Table 3 lists all the emission lines likely produced in this material which were included in the fit, both in the RGS and in the EPIC pn spectra. All the linewidths are unresolved, so they are assumed to be δ functions. Along with lines identified with H-like emission from N, O, Ne, Mg and Si, lines compatible with blends of He-like complexes of the same ionic species are detected. However, the EPIC pn moderate energy resolution does not allow us to resolve any of them, while only the O VII, Ne IX and Mg XI systems are actually separated into their forbidden and resonant components in the RGS spectra. In these cases (also tentatively taking into account the EPIC pn centroid energies of the blends), the results suggest an important role of the forbidden line, which is usually interpreted as the signature of emission predominantly from photoionized rather than collisional plasmas (e.g. Porquet & Dubau 2000). Moreover, the very presence of the O VII and O VIII radiative recombination continua (RRC) argues against a collisional plasma, because in that case this feature would be much broader and very difficult to detect (Liedahl & Paerels 1996; Liedahl 1999).

In the *Chandra* HETG data, some of the He-like complexes are resolved, showing possibly a larger contribution from the resonant line (except for O VII) that was interpreted in terms of photoexcitation of resonant transitions, expected to occur in photoionized plasmas (Sako et al. 2000). These authors argued against the presence of an additional collisionally ionized plasma component (which could explain the anomalous strong resonance lines) because strong Fe L-shell emission is lacking, a result which appears to be confirmed by the *XMM–Newton* spectrum.

Therefore, plasma diagnostics with both *Chandra* and *XMM–Newton* seem to confirm that emission from a photoionized material dominates the soft X-ray spectrum of Mrk 3. The

Table 3. List of the emission lines originating from an ionized material included in the best-fitting model, along with their fluxes and their likely identifications (see text for details).

EPIC pn		RGS			
Energy (keV)	Flux[a]	Energy (keV)	Flux[a]	Id.	E_T[b] (keV)
–	–	$0.43^{+0.03}_{-0.02}$	$2.7^{+1.9}_{-1.2}$	N VI Kα	0.420 (f) 0.426 (i) 0.431 (r)
–	–	$0.50^{+0.02}_{-0.03}$	$1.4^{+1.2}_{-0.4}$	N VII Kα	0.500
$0.565^{+0.003}_{-0.004}$	$14.4^{+1.0}_{-0.8}$	0.562 ± 0.001	$6.3^{+1.3}_{-2.2}$	O VII Kα	0.561 (f)
		0.57 ± 0.01	$2.5^{+1.4}_{-1.3}$	O VII Kα	0.569 (i)
					0.574 (r)
$0.661^{+0.005}_{-0.004}$	$6.2^{+0.5}_{-0.4}$	0.655 ± 0.005	$3.2^{+0.6}_{-0.8}$	O VIII Kα	0.654
		0.666[c]	$0.5^{+0.7}_{-0.4}$	O VII Kβ	0.666
$0.735^{+0.005}_{-0.006}$	$3.7^{+0.5}_{-0.3}$	$0.741^{+0.005}_{-0.008}$	$2.8^{+0.7}_{-1.1}$	O VII RRC	>0.739
$0.780^{+0.009}_{-0.011}$	$1.9^{+0.4}_{-0.3}$	0.775[c]	$0.8^{+0.4}_{-0.7}$	O VIII Kβ	0.775
0.822 ± 0.006	3.2 ± 0.3	0.827 ± 0.002	$1.1^{+0.7}_{-0.3}$	Fe XVII L	0.826
$0.904^{+0.003}_{-0.002}$	6.4 ± 0.3	$0.88^{+0.01}_{-0.02}$	1.6 ± 0.4	O VIII RRC	>0.871
		$0.91^{+0.01}_{-0.03}$	$1.8^{+0.4}_{-0.8}$	Ne IX Kα	0.905 (f)
					0.915 (i)
		0.924 ± 0.002	$1.8^{+0.4}_{-1.0}$	Ne IX Kα	0.922 (r)
0.973 ± 0.009	$1.4^{+0.3}_{-0.2}$	$1.00^{+0.01}_{-0.02}$	$1.4^{+0.5}_{-0.8}$	Fe XX L	0.965
				Fe XXI L	1.009
1.031 ± 0.005	2.5 ± 0.2	$1.02^{+0.05}_{-0.01}$	$1.9^{+0.4}_{-0.9}$	Ne X Kα	1.022
$1.09^{+0.02}_{-0.03}$	0.4 ± 0.2	$1.08^{+0.01}_{-0.03}$	$1.0^{+0.8}_{-0.6}$	Fe XXII L	1.053
$1.10^{+0.02}_{-0.01}$	$0.6^{+0.2}_{-0.1}$	1.128[c]	<0.5	Fe XXIII L	1.128
1.16 ± 0.01	$0.9^{+0.2}_{-0.1}$	1.170[c]	$0.8^{+0.8}_{-0.4}$	Fe XXIV L	1.170
$1.215^{+0.010}_{-0.007}$	1.0 ± 0.1	$1.24^{+0.02}_{-0.04}$	$0.8^{+0.6}_{-0.3}$	Ne X Kβ	1.211
$1.316^{+0.007}_{-0.006}$	1.3 ± 0.1	$1.34^{+0.01}_{-0.04}$	$0.8^{+0.7}_{-0.3}$	Mg XI Kα	1.331 (f)
					1.344 (i)
		$1.36^{+0.03}_{-0.04}$	$0.7^{+0.7}_{-0.3}$	Mg XI Kα	1.352 (r)
1.44 ± 0.01	0.7 ± 0.1	$1.47^{+0.01}_{-0.02}$	$0.8^{+0.8}_{-0.4}$	Mg XII Kα	1.472
$1.57^{+0.02}_{-0.03}$	0.3 ± 0.1	–	–	Mg XI Kβ	1.578
$1.866^{+0.012}_{-0.003}$	0.6 ± 0.1	–	–	Si XIII Kα	1.840 (f)
					1.855 (i)
					1.865 (r)
$1.99^{+0.03}_{-0.02}$	0.2 ± 0.1	–	–	Si XIV Kα	2.005
$2.37^{+0.04}_{-0.03}$	0.4 ± 0.1	–	–	Si XIV Kβ	2.376

[a] 10^{-5} photon cm^{-2} s^{-1}.
[b] Theoretical energies for the transitions. For He-like ions, forbidden, intercombination and resonant lines are separately listed, while the photoionization threshold is listed in the case of RRC (data from NIST; Ralchenko et al. 2004, and references therein).
[c] Fixed.

Table 4. List of the emission lines included in the best-fitting model, originating from a highly ionized material.

Energy (keV)	Flux[a]	Id.	E_T[b] (keV)
			6.637 (f)
$6.71^{+0.03}_{-0.02}$	0.4 ± 0.2	Fe XXV Kα	6.675 (i)
			6.700 (r)
6.97*	<0.1	Fe XXVI Kα	6.966
7.60 ± 0.05	$0.4^{+0.1}_{-0.2}$	Ni XXI–XXIV Kα	7.550–7.668

[a] 10^{-5} photon cm^{-2} s^{-1}.
[b] Theoretical energies for the transitions. For He-like ions, forbidden, intercombination and resonant lines are separately listed (data from NIST; Ralchenko et al. 2004, and references therein).
[c] Fixed.

(tentative) difference between the role of forbidden and resonance lines in the two spectra may be due to the spatial resolution of the two instruments, which could also play a relevant role, given that the *Chandra* observation showed extended emission which is not spatially resolved by *XMM–Newton*. The *XMM–Newton* data might simply indicate the importance of photoionization not only in the innermost nuclear region (as shown by *Chandra* data) but also at larger radii, corresponding to the extended emission revealed by *Chandra*. In the nucleus, low column densities may be the origin of stronger resonant lines, while larger column densities in the extended region could be responsible for predominant forbidden lines (see, for example, Bianchi et al. 2005, for a full discussion on the relative role of the He-like transitions as a function of the column density).

4.2.2 *Ionized iron lines*

An Fe XXV Kα line is required in the EPIC pn spectrum, with a centroid energy of $6.71^{+0.03}_{-0.02}$ keV (see Table 4). This line is actually composed of four transitions, the resonance line (w; 6.700 keV), two intercombination lines (x and y; mean energy 6.675 keV) and the forbidden line (z; 6.637 keV). The best-fitting energy in our data suggests that the dominant transition is the resonance w. This is generally taken as a sign that the gas is mainly in collisional equilibrium (see, for example, Porquet & Dubau 2000). However, the w line can be significantly enhanced by resonant scattering, which is expected to occur in photoionized plasma. This process is very effective at low column densities and the resulting resonance line becomes strongest in the He-like iron spectrum (see, for example, Matt et al. 1996; Bianchi et al. 2005, and references therein). In NGC 1068, the Fe XXV w and z lines were actually resolved and the large ratio between the former to the latter allowed Bianchi et al. (2005) to estimate a column density of a few $\times\ 10^{21}$ cm^{-2}. A similar estimate can be made for Mrk 3, if the centroid energy of the blend of the He-like iron lines is indeed interpreted as the result of a dominant w line.

A line from highly ionized Ni is also detected, possibly associated with the same reflector, while we only found an upper limit for an Fe XXVI line (see Table 3). A much stronger He-like iron line suggests that the ionization parameter of the gas is likely lower than $\log U_x \simeq -0.5$ (see Bianchi et al. 2005, for details). On the other hand, the ionization parameter appropriate for the observed Fe XXV is much higher than that consistent with the production of the other lines found in the soft X-ray spectrum, requiring at least two different ionized reflecting materials in the circumnuclear region of Mrk 3, similarly to what was found, for example, for NGC 1068 (Matt et al. 2004, and references therein).

5 IXO 30

As shown in Fig. 5, a bright source is apparent $\simeq$1.6 arcmin south-east of the nucleus. The much better astrometry of *Chandra* allows us to locate it at $\alpha_{2000} = 06^{\rm h}15^{\rm m}15^{\rm s}$, $\delta_{2000} = +71^\circ02'05''$, fully consistent with *ROSAT* source IXO 30 (Colbert & Ptak 2002).

This source was first detected by *ROSAT* and discussed by Turner et al. (1993) and Morse et al. (1995). We present here the first X-ray spectrum for IXO 30. A combined pn–MOS fit with a simple absorbed power law leads to an acceptable fit ($\chi^2 = 86/75$ d.o.f.), but the addition of an unresolved ($\sigma < 600$ eV) Gaussian line at $6.5^{+0.3}_{-0.2}$ keV is required at the 97 per cent confidence level, according to the F-test. The flux of this feature, likely identified as an iron line, even if the large errors prevent us from stating whether it is ionized or not, is $(8 \pm 6) \times 10^{-7}$ photon cm^{-2} s^{-1}, corresponding to a very large EW of 1.0 ± 0.8 keV. The final fit is good ($\chi^2 = 76/72$ d.o.f.), with $N_{\rm H} = (1.7 \pm 0.4) \times 10^{21}$ cm^{-2} and $\Gamma = 1.77^{+0.13}_{-0.10}$ (see

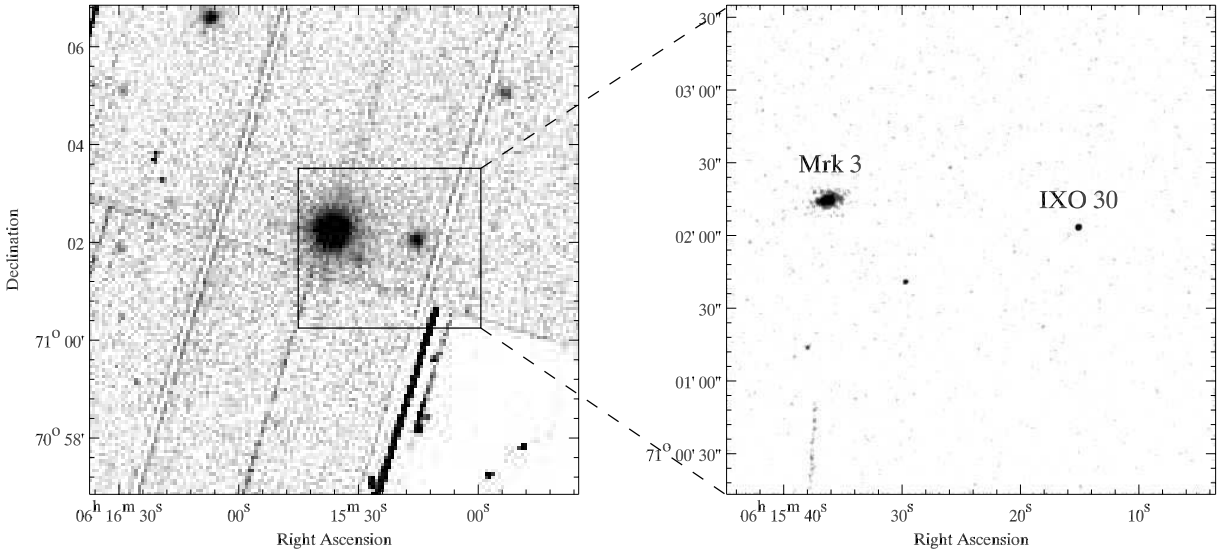

Figure 5. Left: EPIC pn image of the Mrk 3 field. Right: *Chandra* image of the rectangular region shown on the left, together with the identification of Mrk 3 and IXO 30.

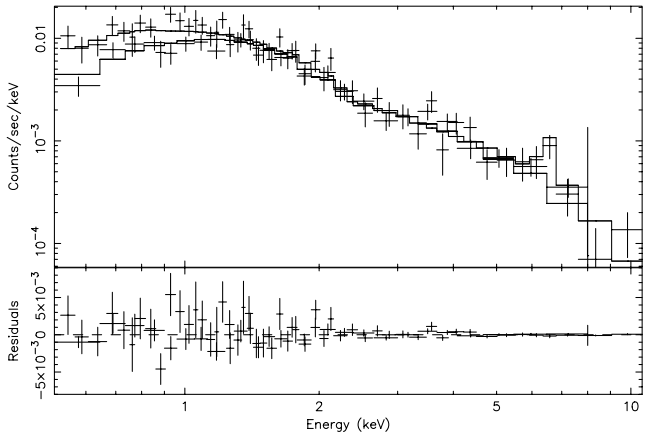

Figure 6. The EPIC pn and MOS1+MOS2 spectrum, best-fitting model and residuals for IXO 30.

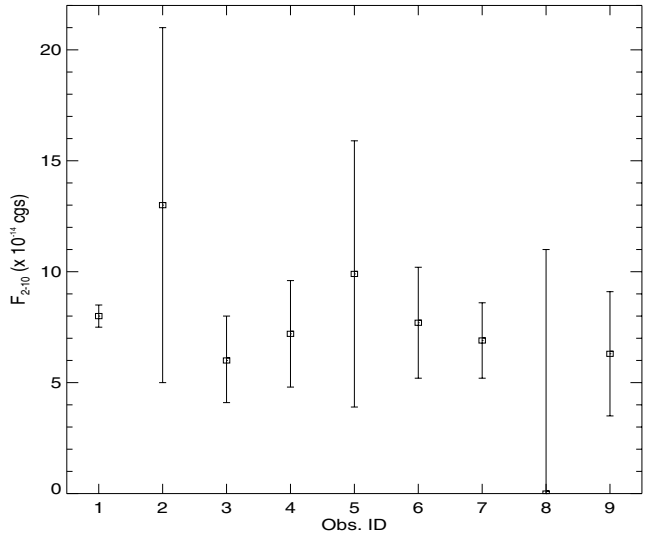

Figure 7. The history of the observed flux of IXO 30 among the available EPIC pn observations (listed in Table 5). All spectra were fitted with an absorbed power law, adopting the best-fitting values of the longest observation.

Fig. 6). A fit of comparable quality ($\chi^2 = 77/73$ d.o.f.) is achieved by a bremsstrahlung component at a temperature of $7.5^{+2.1}_{-1.6}$ keV, absorbed only by the Galactic column density, plus an iron line with the same properties as for the previous model. Finally, we have also tried a single-temperature plasma component (model MEKAL, assuming solar metallicity) that gives a good fit ($\chi^2 = 83/76$ d.o.f.) with a temperature, $8.2^{+1.9}_{-1.2}$ keV, which is enough to take into account the iron line without any further component.

The observed 2–10 keV flux (for all the models) is $\simeq 8.5 \times 10^{-14}$ erg cm^{-2} s^{-1}, corresponding to a luminosity of around 3.5×10^{40} erg s^{-1}, if IXO 30 lies at the same distance of Mrk 3, in good agreement with what was reported by Turner et al. (1993) for the *ROSAT* observation. We found a somewhat higher flux, $\simeq 1.2 \times 10^{-13}$ erg s^{-1}, in the *Chandra* spectrum of the source, but the fit parameters are loosely constrained by the poor statistics, being $N_{\rm H} = (1.9^{+1.8}_{-1.1}) \times 10^{21}$ cm^{-2} and $\Gamma = 1.9^{+0.4}_{-0.3}$ for the power-law model, with an upper limit of 1.3 keV to the EW of the iron line. On the other hand, the analysis of all the available EPIC pn observations does not display any significant variability of the source flux within a time-span of almost 2 yr (see Fig. 7 and Table 5). However,

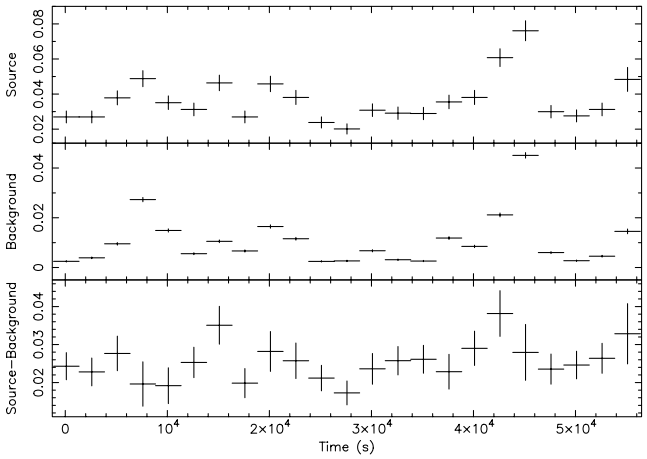

Figure 8. Upper: light curve of the adopted extraction region for IXO 30. Middle: light curve for the background, with count rates rescaled to the area of the source extraction region. Lower: background-subtracted light curve of IXO 30.

Table 5. Log of all the EPIC pn observations of IXO 30 analysed in this paper (see text for details).

Obs. ID	Date	Exp. Time (ks)
1	2000 October 19	53
2	2001 March 12	2
3	2001 March 20	10
4	2001 March 28	5
5	2001 April 05	3
6	2002 March 10	5
7	2002 March 25	5
8	2002 April 18	1
9	2002 September 16	5

it is interesting to note that the only observation long enough to allow some spectral analysis (observation 3 in Table 5) suggests a possible variation of the absorbing column density, because a larger value, $N_{\rm H} = 7.2^{+4.9}_{-3.6} \times 10^{21}$ cm^{-2}, is required by the data. Finally, no clear evidence for short-term variability is present in the EPIC pn light curve of IXO 30 (see Fig. 8), considering that the high background periods (filtered for the extraction of the spectra) are comparable to the source flux and are not easily subtracted from the light curve.

We have searched for an optical counterpart of IXO 30 in the Digitized Sky Survey, but we have not found any possible companion either in the POSS-II Red or in the Blue plate, thus implying that the source is fainter than $R \simeq 21$ and $B_{\rm J} \simeq 22.5$. It is therefore quite difficult to guess its real nature. A possible interpretation is in terms of an AGN, which must be a background object, otherwise its luminosity would be too low. In any case, the presence of an iron line allows us to put an upper limit on the redshift of the source, assuming that the line comes from H-like iron; this limit, being approximately $z < 0.1$, implies that the 2–10 keV flux of the source cannot be larger than $\simeq 2 \times 10^{42}$ erg s^{-1}, quite low for an AGN. Moreover, the EW of the iron line, although determined with large uncertainty, would be typical of a Compton-thick object, but this would be at odds with the observed photon index. On the other hand, if associated with the Mrk 3 galaxy, its luminosity is comparable with that usually found for ultraluminous X-ray sources (ULXs) often detected in the

vicinity of an AGN and possibly related to intermediate-mass BHs (see, for example, Colbert & Miller 2005). If the latter interpretation is correct, at least a mass of $\simeq$300 $M_\odot$ is required, if the source is emitting near the Eddington limit. However, the origin of the huge iron line remains obscure, even if at least another ULX was recently found in M82, showing a similar feature (Strohmayer & Mushotzky 2003). Furthermore, a separation of 1.6 arcmin at the redshift of Mrk 3 would imply a large distance ($\simeq$25 kpc) of the source from the nucleus, which is very close to the optical D_{25} diameter of the host galaxy (de Vaucouleurs et al. 1991). Thus, the probability of contamination from background/foreground objects is significant (see, for example, Ptak & Colbert 2004).

Finally, an interpretation in terms of a Galactic source, probably a cataclysmic variable (CV), is possible. This scenario is favoured by the spectral analysis, because a bremsstrahlung component and a huge iron line are generally the main ingredients to model these objects (see, for example, Mukai & Shiokawa 1993). At a distance of $\simeq$500 pc from the Earth, a 2–10 keV luminosity of $\simeq 2 \times 10^{30}$ erg s^{-1} would make IXO 30 a weak CV, but still in the observed range (see, for example, Mukai & Shiokawa 1993). On the other hand, if we assume, as is generally found, that the secondary of this system is a typical M red dwarf, we can obtain a lower limit on the distance of the CV, based on the upper limit we have on its apparent R magnitude. The resulting distance, approximately $d > 4$ kpc, is in agreement with an origin of the source in the Galactic disc, also taking into account its Galactic coordinates. This would imply a 2–10 keV luminosity larger than 10^{32} erg s^{-1}, which is within the observed range in CVs.

6 CONCLUSIONS

We have analysed the first *XMM–Newton* spectrum of Mrk 3. The analysis confirms previous results, showing a spectrum composed by three main components: a strongly absorbed power law, a pure Compton reflection with the same photon index associated with an iron Kα line, both produced as reflection from a Compton-thick torus, and an unabsorbed power law, again with the same photon index as the primary continuum, associated with a large number of emission lines, likely produced as reflection from a Compton-thin, photoionized material.

The iron Kα line EW with respect to the Compton reflection component, being only 610^{+30}_{-50} eV, is consistent with a low inclination angle and an iron underabundance of a factor of $\simeq$0.82, properties independently derived for the torus, via the amount of Compton reflection and the depth of the iron edge. Moreover, the iron linewidth is actually resolved in the EPIC pn spectrum, with $\sigma = 32^{+13}_{-14}$ eV, corresponding to FWHM $= 3500^{+1400}_{-1500}$ km s^{-1} if produced by Doppler broadening, thus putting an estimate to the inner radius of the torus, $r = 0.6^{+1.3}_{-0.3}$ sin^2 i pc. On the other hand, a possible variation on a time-scale of $\simeq$ seven months of the ionization stage of iron between the *Chandra* and the *XMM–Newton* observations is fully compatible with the photoionization time for iron at a distance of around 1 pc.

The soft X-ray spectrum of Mrk 3 is dominated by H- and He-like emission lines from the most abundant metals, superimposed over an unabsorbed power law with the same photon index of the primary continuum. It is important to note that the full resolution of these lines in the RGS spectra was required before correctly fitting this part of the spectrum in the lower-resolution pn data, thus preventing the adoption of a much steeper ($\Gamma \simeq 3$) power law, whose physical interpretation would have been less straightforward. From the ratio between the fluxes of the reflected component and the primary continuum, a column density of a few $\times 10^{22}$ cm^{-2} can be derived for the photoionized material. However, it must be noted that at least two different ionized reflectors are needed to take into account the emission lines from lighter metals and the Fe XXV emission line at $6.71^{+0.03}_{-0.02}$ keV.

We have also presented the first X-ray spectrum of *ROSAT* source IXO 30, which shows a huge iron line at $6.5^{+0.3}_{-0.2}$ keV and is well represented either by an absorbed power law with $\Gamma \simeq 1.8$ or bremsstrahlung emission at a temperature of $7.5^{+2.1}_{-1.6}$ keV. Even if the lack of any optical counterpart precludes excluding other possibilities, such as a ULX at the distance of Mrk 3, its spectral properties point to a likely identification in terms of a Galactic CV.

ACKNOWLEDGMENTS

We would like to thank G. Matt and M. Guainazzi for many useful discussions, and the referee for his valuable comments. SB acknowledges Fondazione Della Riccia for some financial support. GM and KI thank the UK Particle Physics and Astronomy Research Council (PPARC) for support. ACF thanks the Royal Society for support. This paper is based on observations obtained with *XMM–Newton*, a European Space Agency (ESA) science mission with instruments and contributions directly funded by ESA Member States and the USA (NASA). The Digitized Sky Survey was produced at the Space Telescope Science Institute under US Government grant NAG W-2166. The images of these surveys are based on photographic data obtained using the Oschin Schmidt Telescope on Palomar Mountain and the UK Schmidt Telescope.

REFERENCES

Anders E., Grevesse N., 1989, Geochim. Cosmochim. Acta, 53, 197
Awaki H., Koyama K., Kunieda H., Tawara Y., 1990, Nat, 346, 544
Awaki H., Koyama K., Inoue H., Halpern J. P., 1991, PASJ, 43, 195
Basko M. M., 1978, ApJ, 223, 268
Bearden J. A., 1967, Rev. Mod. Phys., 39, 78
Bianchi S., Matt G., Fiore F., Fabian A. C., Iwasawa K., Nicastro F., 2002, A&A, 396, 793
Bianchi S., Matt G., Nicastro F., Porquet D., Dubau J., 2005, MNRAS, 357, 599
Cappi M. et al., 1999, A&A, 344, 857
Colbert E. J. M., Miller M. C., 2005, in Novello M., Perez-Bergliaffa S., Ruffini R., eds, Invited review talk at the 10th Marcel Grossmann Meeting on General Relativity. World Scientific, Singapore, in press (astro-ph/0402677)
Colbert E. J. M., Ptak A. F., 2002, ApJS, 143, 25
de Vaucouleurs G., de Vaucouleurs A., Corwin H. G., Buta R. J., Paturel G., Fouque P., 1991, Third Reference Catalogue of Bright Galaxies. Springer-Verlag, Berlin
Dickey J. M., Lockman F. J., 1990, ARA&A, 28, 215
Ehle M. et al., 2003, *XMM–Newton* User's Handbook, http://xmm.vilspa.esa.es/external/xmm_user_support/documentation/uhb_2.1
Georgantopoulos I., Papadakis I., Warwick R. S., Smith D. A., Stewart G. C., Griffiths R. G., 1999, MNRAS, 307, 815
Guainazzi M., Rodriguez-Pascual P., Fabian A. C., Iwasawa K., Matt G., 2004, MNRAS, 355, 297
House L. L., 1969, ApJS, 18, 21
Iwasawa K., Yaqoob T., Awaki H., Ogasaka Y., 1994, PASJ, 46, L167
Iwasawa K., Maloney P. R., Fabian A. C., 2002, MNRAS, 336, L71
Kaastra J. S., Mewe R., 1993, A&AS, 97, 443
Kruper J. S., Canizares C. R., Urry C. M., 1990, ApJS, 74, 347

Liedahl D. A., 1999, in van Paradijs J., Bleeker J. A. M., eds, X-Ray Spectroscopy in Astrophysics, Lecture Notes in Physics Vol. 520. Springer-Verlag, Berlin, p. 189
Liedahl D. A., Paerels F., 1996, ApJ, 468, L33
Magdziarz P., Zdziarski A. A., 1995, MNRAS, 273, 837
Matt G., 2002, MNRAS, 337, 147
Matt G., Brandt W. N., Fabian A. C., 1996, MNRAS, 280, 823
Matt G., Bianchi S., Guainazzi M., Molendi S., 2004, A&A, 414, 155
Miller J. S., Goodrich R. W., 1990, ApJ, 355, 456
Molendi S., Bianchi S., Matt G., 2003, MNRAS, 343, L1
Morse J. A., Wilson A. S., Elvis M., Weaver K. A., 1995, ApJ, 439, 121
Mukai K., Shiokawa K., 1993, ApJ, 418, 863
Ogle P. M., Brookings T., Canizares C. R., Lee J. C., Marshall H. L., 2003, A&A, 402, 849
Palmeri P., Mendoza C., Kallman T. R., Bautista M. A., Meléndez M., 2003, A&A, 410, 359
Piconcelli E., Jimenez-Bailón E., Guainazzi M., Schartel N., Rodríguez-Pascual P. M., Santos-Lleó M., 2004, MNRAS, 351, 161
Porquet D., Dubau J., 2000, A&AS, 143, 495
Ptak A., Colbert E., 2004, ApJ, 606, 291
Ralchenko Y., Jou F.-C., Kelleher D. E., Kramida A. E., Musgrove A., Reader J., Wiese W., Olsen K., 2004, NIST Atomic Spectra Database, version 3.0-beta. National Institute of Standards and Technology, Gaithersburg, MD (available at http://physics.nist.gov/asd3)
Reynolds C. S., Fabian A. C., Nandra K., Inoue H., Kunieda H., Iwasawa K., 1995, MNRAS, 277, 901
Sako M., Kahn S. M., Paerels F., Liedahl D. A., 2000, ApJ, 543, L115
Strohmayer T. E., Mushotzky R. F., 2003, ApJ, 586, L61
Strüder L. et al., 2001, A&A, 365, L18
Tran H. D., 1995, ApJ, 440, 565
Turner T. J., Urry C. M., Mushotzky R. F., 1993, ApJ, 418, 653
Turner M. J. L. et al., 2001, A&A, 365, L27
Verner D. A., Yakovlev D. G., 1995, A&AS, 109, 125
Woo J., Urry C. M., 2002, ApJ, 579, 530
Yaqoob T., George I. M., Nandra K., Turner T. J., Serlemitsos P. J., Mushotzky R. F., 2001, ApJ, 546, 759

This paper has been typeset from a TEX/LATEX file prepared by the author.